



Analysis of the potential for non-invasive imaging of oxygenation at heart depth, using ultrasound optical tomography (UOT) or photo-acoustic tomography (PAT)

ANDREAS WALTHER,^{1,*} LARS RIPPE,¹ LIHONG V. WANG,²
STEFAN ANDERSSON-ENGELS,^{3,4} AND STEFAN KRÖLL¹

¹Department of Physics, Lund University, 221 00 Lund, Sweden

²California Institute of Technology, 1200 E California Blvd., MC 138-78, Pasadena CA 91125, USA

³Tyndall National Institute, Lee Maltings, Dyke Parade, Cork, T12 R5CP, Ireland

⁴Department of Physics, University College Cork, Cork, Ireland

*andreas.walther@fysik.lth.se

Abstract: Despite the important medical implications, it is currently an open task to find optical non-invasive techniques that can image deep organs in humans. Addressing this, photo-acoustic tomography (PAT) has received a great deal of attention in the past decade, owing to favorable properties like high contrast and high spatial resolution. However, even with optimal components PAT cannot penetrate beyond a few centimeters, which still presents an important limitation of the technique. Here, we calculate the absorption contrast levels for PAT and for ultrasound optical tomography (UOT) and compare them to their relevant noise sources as a function of imaging depth. The results indicate that a new development in optical filters, based on rare-earth-ion crystals, can push the UOT technique significantly ahead of PAT. Such filters allow the contrast-to-noise ratio for UOT to be up to three orders of magnitude better than for PAT at depths of a few cm into the tissue. It also translates into a significant increase of the image depth of UOT compared to PAT, enabling deep organs to be imaged in humans in real time. Furthermore, such spectral holeburning filters are not sensitive to speckle decorrelation from the tissue and can operate at nearly any angle of incident light, allowing good light collection. We theoretically demonstrate the improved performance in the medically important case of non-invasive optical imaging of the oxygenation level of the frontal part of the human myocardial tissue. Our results indicate that further studies on UOT are of interest and that the technique may have large impact on future directions of biomedical optics.

© 2017 Optical Society of America

OCIS codes: (110.0113) Imaging through turbid media; (170.3880) Medical and biological imaging; (160.5690) Rare-earth-doped materials.

References and links

1. Personal communication with Lars Edvinsson, Chief Senior Consultant, Lund University Hospital.
2. M. G. Friedrich and T. D. Karamitsos, "Oxygenation-sensitive cardiovascular magnetic resonance," *Journal of Cardiovascular Magnetic Resonance* **15**, 1–11 (2013).
3. A. Taruttis and V. Ntziachristos, "Advances in real-time multispectral optoacoustic imaging and its applications," *Nature Photon.* **9**, 219–227 (2015).
4. D. S. Elson, R. Li, C. Dunsby, R. Eckersley, and M.-X. Tang, "Ultrasound-mediated optical tomography: a review of current methods," *Interface Focus* **1**, 632–648 (2011).
5. C. Kim, T. N. Erpelding, L. Jankovic, M. D. Pashley, and L. V. Wang, "Deeply penetrating in vivo photoacoustic imaging using a clinical ultrasound array system," *Biomed. Opt. Express* **1**, 278–284 (2010).
6. J. Yao, L. Wang, J.-M. Yang, K. I. Maslov, T. T. W. Wong, L. Li, C.-H. Huang, J. Zou, and L. V. Wang, "High-speed label-free functional photoacoustic microscopy of mouse brain in action," *Nature Methods* **12**, 407–410 (2015).
7. A. Hussain, W. Petersen, J. Staley, E. Hondebrink, and W. Steenbergen, "Quantitative blood oxygen saturation imaging using combined photoacoustics and acousto-optics," *Opt. Lett.* **41**, 1720–1723 (2016).
8. L. V. Wang and J. Yao, "A practical guide to photoacoustic tomography in the life sciences," *Nat Meth* **13**, 627–638 (2016).

9. B. T. Cox, J. G. Laufer, P. C. Beard, and S. R. Arridge, "Quantitative spectroscopic photoacoustic imaging: a review," *J. Biomed. Opt.* **17**, 061202 (2012).
10. M. Gross, P. Goy, and M. Al-Koussa, "Shot-noise detection of ultrasound-tagged photons in ultrasound-modulated optical imaging," *Opt. Lett.* **28**, 2482–2484 (2003).
11. S. Resink, E. Hondebrink, and W. Steenbergen, "Solving the speckle decorrelation challenge in acousto-optic sensing using tandem nanosecond pulses within the ultrasound period," *Opt. Lett.* **39**, 6486–6489 (2014).
12. H. Zhang, M. Sabooni, L. Rippe, C. Kim, S. Kröll, L. V. Wang, and P. R. Hemmer, "Slow light for deep tissue imaging with ultrasound modulation," *Appl. Phys. Lett.* **100**, 131102 (2012).
13. M. S. Patterson, E. Schwartz, and B. C. Wilson, "Quantitative reflectance spectrophotometry for the noninvasive measurement of photosensitizer concentration in tissue during photodynamic therapy," *Proc. SPIE* **1065**, 115–122 (1989).
14. R. C. Haskell, L. O. Svaasand, T.-T. Tsay, T.-C. Feng, M. S. McAdams, and B. J. Tromberg, "Boundary conditions for the diffusion equation in radiative transfer," *J. Opt. Soc. Am. A* **11**, 2727–2741 (1994).
15. American National Standard for Safe Use of Lasers, ANSI Z136.1.
16. M. Jang, H. Ruan, B. Judkewitz, and C. Yang, "Model for estimating the penetration depth limit of the time-reversed ultrasonically encoded optical focusing technique," *Opt. Express* **22**, 5787–5807 (2014).
17. L. Wang, G. Li, J. Xia, and L. V. Wang, "Ultrasonic-heating-encoded photoacoustic tomography with virtually augmented detection view," *Optica* **2**, 307–312 (2015).
18. A. M. Winkler, K. Maslov, and L. V. Wang, "Noise-equivalent sensitivity of photoacoustics," *J. Biomed. Opt.* **18**, 097003 (2013).
19. A. Petschke and P. J. La Riviere, "Comparison of intensity-modulated continuous-wave lasers with a chirped modulation frequency to pulsed lasers for photoacoustic imaging applications," *Biomed. Opt. Express* **1**, 1188–1195 (2010).
20. R. Horstmeyer, H. Ruan, and C. Yang, "Guidestar-assisted wavefront-shaping methods for focusing light into biological tissue," *Nature Photon.* **9**, 563–571 (2015).
21. B. Jayet, J.-P. Huignard, and F. Ramaz, "Optical phase conjugation in Nd:YVO₄ for acousto-optic detection in scattering media," *Opt. Lett.* **38**, 1256–1258 (2013).
22. S. J. Matcher, M. Cope, and D. T. Delpy, "In vivo measurements of the wavelength dependence of tissue-scattering coefficients between 760 and 900 nm measured with time-resolved spectroscopy," *Appl. Opt.* **36**, 386–396 (1997).
23. A. Torricelli, A. Pifferi, P. Taroni, E. Giambattistelli, and R. Cubeddu, "In vivo optical characterization of human tissues from 610 to 1010 nm by time-resolved reflectance spectroscopy," *Phys. Med. Biol.* **46**, 2227–2237 (2001).
24. P. Taroni, A. Pifferi, A. Torricelli, D. Comelli, and R. Cubeddu, "In vivo absorption and scattering spectroscopy of biological tissues," *Photochem. Photobiol. Sci.* **2**, 124–129 (2003).
25. I. J. Bigio and S. Fantini, *Quantitative Biomedical Optics: Theory, Methods, and Applications* (Cambridge University Press, 2016).
26. S. L. Jacques, "Optical properties of biological tissues: a review," *Phys. Med. Biol.* **58**, R37–R61 (2013).
27. T. Svensson, J. Swartling, P. Taroni, A. Torricelli, P. Lindblom, C. Ingvar, and S. Andersson-Engels, "Characterization of normal breast tissue heterogeneity using time-resolved near-infrared spectroscopy," *Phys. Med. Biol.* **50**, 2559–2571 (2005).
28. R. W. Equall, Y. Sun, R. L. Cone, and R. M. Macfarlane, "Ultraslow optical dephasing in $Eu^{3+} : Y_2SiO_5$," *Phys. Rev. Lett.* **72**, 2179–2181 (1994).
29. Y. Sun, C. W. Thiel, R. L. Cone, R. W. Equall, and R. L. Hutcheson, "Recent progress in developing new rare earth materials for hole burning and coherent transient applications," *J. Lumin.* **98**, 281–287 (2002).
30. M. Nilsson, L. Rippe, R. Klieber, D. Suter, and S. Kröll, "Holeburning techniques for isolation and study of individual hyperfine transitions in inhomogeneously broadened solids, demonstrated in $Pr^{3+}Y_2SiO_5$," *Phys. Rev. B* **70**, 214116 (2004).
31. F. Könz, Y. Sun, C. W. Thiel, R. L. Cone, R. W. Equall, R. L. Hutcheson, and R. M. Macfarlane, "Temperature and concentration dependence of optical dephasing, spectral-hole lifetime, and anisotropic absorption in $Eu^{3+}Y_2SiO_5$," *Phys. Rev. B* **68**, 085109 (2003).
32. S. E. Beavan, E. A. Goldschmidt, and M. J. Sellars, "Demonstration of a dynamic bandpass frequency filter in a rare-earth ion-doped crystal," *J. Opt. Soc. Am. B* **30**, 1173–1177 (2013).
33. A. Kinos, Q. Li, L. Rippe, and S. Kröll, "Development and characterization of high suppression and high etendue narrowband spectral filters," *Appl. Opt.* **55**, 10442–10448 (2016).
34. M. Sabooni, A. N. Nilsson, G. Kristensson, and L. Rippe, "Wave propagation in birefringent materials with off-axis absorption or gain," *Phys. Rev. A* **93**, 013842 (2016).
35. C. Clausen, F. Bussi eres, M. Afzelius, and N. Gisin, "Quantum storage of heralded polarization qubits in birefringent and anisotropically absorbing materials," *Phys. Rev. Lett.* **108**, 190503 (2012).
36. A. Walther, A. Amari, S. Kr  ll, and A. Kalachev, "Experimental superradiance and slow light effects for quantum memories," *Phys. Rev. A* **80**, 012317 (2009).
37. R. N. Shakhmuratov, A. Rebane, P. Megret, and J. Odeurs, "Slow light with persistent hole burning," *Phys. Rev. A* **71**, 053811 (2005).
38. R. L. Ahlefeldt, M. R. Hush, and M. J. Sellars, "Ultrannarrow optical inhomogeneous linewidth in a stoichiometric rare-earth crystal," *Phys. Rev. Lett.* **117**, 250504 (2016).

39. The Matlab code with core calculations <https://doi.org/10.6084/m9.figshare.5178538>.

1. Introduction

Ischemia, restriction of blood and therefore oxygen supply in the body, is one of the most important medical challenges today. Estimations suggest that up to 25% of all cases in the emergency ward in western countries are related to determining ischemia [1], indicating possible severe afflictions such as myocardial infarction, internal bleeding or stroke. One case of ischemia, coronary artery disease which can lead to infarction, is also the most common cause of death in the world.

The clinically most used modalities for the imaging of coronary vessel occlusions, leading to myocardial ischemia, are: X-ray angiography, CT angiography and perfusion Cardiovascular Magnetic Resonance (CMR). They are all indirect methods, e.g. measuring myocardial tissue blood flow or volume, and can thus not measure the actual oxygenation level. In addition they are associated with several drawbacks such as being invasive, requiring contrast agents with potential side effects or delivering high doses of radiation that may increase cancer risks. Non-invasive direct measurements of oxygenation are currently being investigated, including CMR using the Blood Oxygen-Level Dependent (BOLD) scheme [2], Photo-Acoustic Tomography (PAT) [3] and Ultrasound Optical Tomography (UOT) [4]. The BOLD CMR scheme has so far shown limited contrast-to-noise ratios and susceptibility to artifacts [2], in addition to being an expensive and complicated method. Apparatuses based on PAT have recently entered the commercial market, using optical imaging to make it much cheaper and faster than MR-based approaches. However, so far imaging depths are generally limited to a few millimeters up to a centimeter, not deep enough to reach human organs such as the heart, although some experimental studies seem promising [5,6].

Measuring the oxygenation has been demonstrated using both PAT [6] and UOT [7]. For PAT, it remains a challenge to obtain an absolute value [8], but it is possible using multiple wavelengths [9]. While PAT will always be limited by the thermal noise of the tissue, UOT has been shown to allow shot noise limited measurements by using heterodyne techniques [10]. One difficulty here is that phase sensitive techniques are generally sensitive to speckle decorrelation giving very limited measurement times. In general, phase sensitive techniques puts large demands on fast detectors and high computational bandwidth for real time demodulation. A suggestion to overcome the speckle decorrelation was made in Ref. [11], by using a pair of short pulses matched with the ultrasound phase. Another way to achieve shot noise limited measurements is to remove the large background entirely and in this paper we focus on this approach using a new development of narrow-band optical filters based on rare-earth ions. The performance of these filters are not related to the phase of the light in any way, which makes them completely immune to speckle decorrelation due to tissue movement. These rare-earth filters have recently been used to demonstrate UOT through several centimeters of low-blood tissue [12], indicating a high potential for this technique that has yet to be fully explored.

In this paper we perform calculations that demonstrate the potential for UOT to reach higher imaging depths than PAT for strongly scattering tissues. The calculations take into account a realistic set of assumptions and the limiting noise sources are identified for both techniques allowing a general optical performance versus depths to be assessed. Our analysis reveals that a few centimeters into tissue the absorption contrast, and thus also the oxygenation contrast that could be distinguished, is up to three orders of magnitude better for UOT compared to PAT. We then focus on one medically interesting example of imaging the oxygenation of the myocardial tissue. Here, 30 measurement points across the heart should be resolved in real time, i.e. in a time shorter than a heart beat. Calculations show that while PAT can penetrate about 3 cm into tissue in this case, UOT has the potential for double the depth at 6 cm, enough to reach the front

heart muscle (heart wall), where the largest portion of ischemia cases are located. These results show the potential for a new paradigm of optical medical imaging, that may even be extended further by adding wave-front shaping techniques.

2. Theory

2.1. A brief overview of PAT and UOT

Both UOT and PAT are based on sending optical light pulses into tissue, which are then diffusing out in the material due to the high scattering. For PAT, in each location in the tissue the absorbed pulse energy is turned into heat. This heat causes an expansion of the tissue, at a rate that depends on how much energy was absorbed, i.e. it depends on the absorption coefficient that one wants to measure. This expansion then propagates through the material as an acoustic pressure wave, which can be detected at the surface by a microphone. By recording the timing of signals between microphones at different positions, it is possible to reconstruct all regions where the light has been absorbed using only a single excitation pulse.

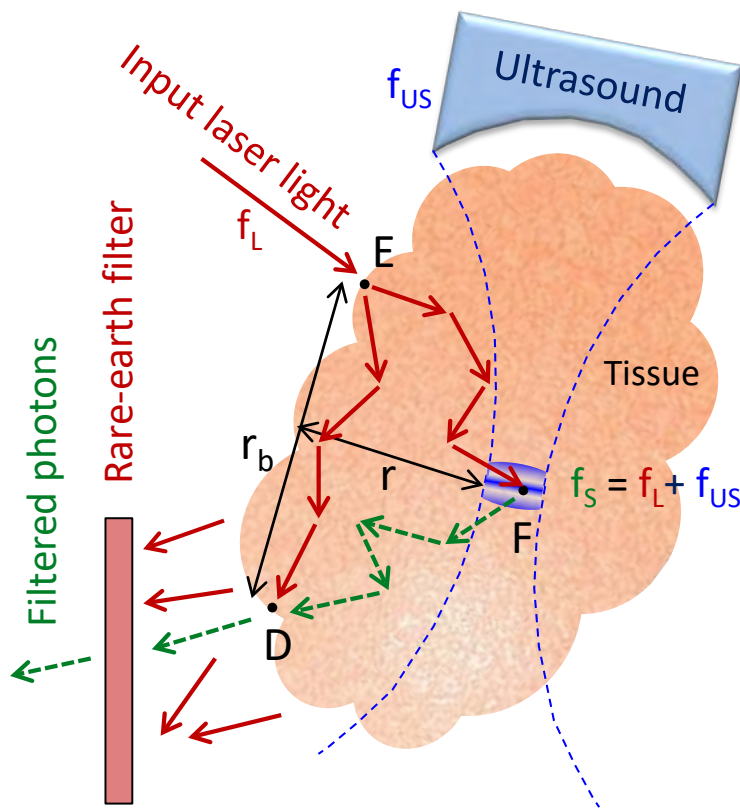


Fig. 1. Overview of the UOT setup. The input laser light takes a random walk path (solid red arrows) towards the ultrasounds focus point, F, where it gets diffracted and receives a frequency shift. After exiting the tissue, the frequency-shifted photons (dashed green arrows) are filtered out from the large background of unshifted photons. The largest contribution of background photons, which did not acquire a frequency shift, have traveled a shorter path from the entry point, E, to the detection point D. The frequency shifted photons detected after the filter carry information that can be localized to the focal spot.

In UOT, by contrast, a single region is selected at the time by using a focused ultrasound pulse.

Ultrasound (US) is used in conventional medical imaging and it can be focused with good spatial resolution since most tissue components have similar acoustic impedance. Light that finds its way into the focal region of the sound wave can be diffracted and then also frequency shifted by the sound. This frequency shifted light propagates out of the tissue and a fraction of this light can be captured by a light detector. If the frequency shifted light can be filtered out from the background, as shown in Fig. 1, it then carries information from the focal region that can be compared to other regions by moving the US focus. For more information see e.g. Ref. [4].

2.2. Theoretical models

Due to the strong scattering in biological tissue, light propagation can be seen as a random walk, or a diffusion process. For a point like source (the entry point of the laser pulse) the light fluence (J/cm^2), ϕ , at a total depth of r_{tot} cm into the tissue can approximately be given by [13]:

$$\phi = N \hbar \omega \cdot \frac{\mu_{eff}^2}{4\pi\mu_a} \frac{1}{r_{tot}} e^{-\mu_{eff} r_{tot}}, \quad (1)$$

where N is the total photon number in the pulse and $\mu_{eff} = \sqrt{3\mu_a(\mu_a + \mu'_s)}$ is the effective attenuation coefficient (and the factor $\mu_a/\mu_{eff}^2 = D$ is also the corresponding diffusion constant). This is composed of the absorption coefficient, μ_a , and the reduced scattering coefficient, μ'_s . These can vary significantly between tissue types, are wavelength dependent, and we will discuss the appropriate choice of them separately in Sec. 4. At the entrance of the tissue there are boundary conditions that affect the propagation [14], but these effects were tested in our calculations and found to be negligible. This was expected since our investigations are on relatively large imaging depths compared to the scattering mean free path.

The number of photons available in each pulse is ultimately restricted by medical safety limits to about $20 \text{ mJ}/\text{cm}^2$ for short pulses and $200 \text{ mW}/\text{cm}^2$ of average radiation [15]. These limits have different effects on the two techniques described, since there are different optimal strategies for maximizing the signal contrast, as we will see in the following subsections. The measurement we aim to investigate is to resolve an absorption contrast, i.e. a difference in absorption coefficients, $\Delta\mu_a = |\mu_{a,signal} - \mu_{a,baseline}|$, between two near-lying volume elements (voxels) in tissue. The two different voxels, *signal* and *baseline*, could e.g. be two regions with different oxygenation levels in the heart, or tumor tissue compared to healthy tissue etc.

As one example in this paper we look at oxygenation levels in the human heart. The oxygenation is related to the absorption difference through a factor that depends on the choice of wavelength, as discussed in Sec. 4. In our calculations we have chosen the main signal to be at a wavelength of 880 nm, where a 1 percent decrease of blood oxygenation level gives a decrease of the absorption coefficient by 0.37 percent. Thus, if the measured signal reveals an absorption change of $\Delta\mu_a/\mu_a$, it can be inferred that the change of oxygen saturation corresponds to:

$$\Delta(\text{O}_2)_{\text{Sat}} = \frac{1}{0.37} \frac{\Delta\mu_a}{\mu_a} \quad (2)$$

The final signal level, described in more detail for UOT and PAT in their subsections below, is essentially related to the absorption coefficient of the chosen region through Beer-Lambert's law: $N_{signal} = N_0 e^{-\mu_{a,signal} d}$. Here, N_0 is the photon number remaining after all other loss sources and should not change significantly between different close-lying regions. This is an assumption which may not always be true, but in our example both regions are close, at the same depth and consist of the same tissue (heart wall), so this assumption should be reasonable. In addition to that, one may employ a measurement on a second wavelength that can be used as a reference. For our suggested technique there is a suitable rare-earth filter available at 790 nm for this purpose (see Sec. 4.2). The parameter d is the distance inside the measurement region traveled by the

light. In a scattering medium this is given by a random walk path of the photons over the size of the region, which in our case is 3 mm giving $d = 4.5$ mm.

In this example, the aim is to calculate the signal levels that can be reached when measuring 30 voxels across the heart. Placing them in a line allows them to roughly cover the length of the heart, given the spatial resolution of about 3 mm. In order to make a fair comparison between the two techniques we will assume a common measurement objective, namely to be able to measure all those 30 regions within a 250 ms time interval. This is an interval over which the heart is roughly stationary during its heart beat cycle. For UOT, this means we can spend 8.33 ms per region, while PAT can obtain a signal from multiple regions at the same time and does not need this division of power. For tissue depths up to 10 cm an ultrasound frequency of about 3 MHz is suitable with a US bandwidth of about 2 MHz. We further assume the same spatial resolution and detector area for both techniques.

2.3. Ultrasound optical tomography (UOT)

As described in the overview above (Sec. 2.1), a spatially selective signal is obtained when the light scatters off of the ultrasound (US) focus, obtaining a frequency shift equal to the US frequency, typically a few MHz. Only a very small fraction of the light enters the region of the US focus and gets diffracted, and in order to use this spatial information, all other photons that did not get frequency shifted will have to be filtered away. Such a filter would need a ratio of potentially more than 60 dB (an intensity factor 10^6), between transmitted and attenuated light although their frequencies would differ only by a few MHz (on a carrier frequency of $>10^{14}$ Hz). The requirement on the filter attenuation is investigated in our work and discussed in Sec. 3 (second to last paragraph). Obtaining a high contrast while allowing arbitrary input angles can e.g. be achieved by spectral programming of rare-earth ions, to be discussed in more detail in Sec. 4B.

The light enters at point E in the Fig. 1 and is finally detected at point D . The spatial region from which we wish to receive information is the US focus, F , and the filters make sure that only light that has passed through this volume is detected. The imaging depth, r , is here defined as the shortest distance from the measuring region F to the surface. This means that in order for the light to reach F , it must diffusely travel from E to F , a distance of $r_{tot} = \sqrt{r^2 + (r_b/2)^2}$, where r_b is the distance between the entry and the detection. The distance r_b can be chosen arbitrarily but should be roughly matched with the targeted imaging depth. Note that there are other similar geometries that would work equally well. The main point of our choice is to, in a simple way, capture the fact that if r_b is made smaller the total depth decreases and the signal thus increases, but at the same time the background light also increases. This creates a trade-off situation and we find that there is an optimum when r_b is roughly matched with the targeted imaging depth.

By moving the US focus to different spatial positions, local changes due to the varying tissue characteristics can be detected. We assume a light diffraction efficiency due to the ultrasound in the order of about 10% (calculated using ref. [16]), which can be readily obtained while staying below the medically allowed US power. The light then propagates out of the tissue again experiencing another loss as given by Eq. (1) with the same r_{tot} as when it went in. At low light levels the detection efficiency can be around 50% for typical low light detectors.

Out of the fluence that reaches a detector of area $A_{det} = 1$ cm², a certain number of signal photons, N_{signal} , remain after the losses from all stages and are detected. These photons have to be sufficiently many that one could detect an absorption contrast between two different types of tissue in the US focus. This could for example be two regions with different oxygenation levels, giving rise to different absorption coefficients. To explore what minimum absorption contrasts that are detectable the signal will be compared with a corresponding photon number, $N_{baseline}$, from the second region. This contrast must be visible on top of the noise level, which is ultimately (at low light levels) given by the shot noise of the total amount of photons,

$N_{total} = N_{signal} + N_{background}$, at the detector. Here, $N_{background}$ is the photons that are diffusely traveling the shallower and shorter distance from the entry point, E , to the detection point, D , in Fig. 1. This term will dominate the total photon count at larger imaging depths. In total, the obtained contrast-to-noise ratio is given by:

$$CNR_{UOT} = \frac{N_{signal} - N_{baseline}}{\sqrt{N_{total}}} \quad (3)$$

As mentioned above, the goal of our example is to be able to measure 30 regions in the heart within the 250 ms stable time interval. This means that the total photon number, which must be compatible with the medical safety limits, will have to be divided between each of those 30 regions. Since CNR_{UOT} is increasing with the total input photon number, it will be optimal to choose the medical safety limit with the highest total number of photons, which in this case is the one for average radiation. Although it does not matter for the CNR, using the slow light filters described in the Sec. 4 requires a pulsed scheme and we find that pulses of about 4 μ s with a repetition rate of 25 kHz work well and can reach the allowed 200 mW/cm² using a 2 W continuous laser.

2.4. Photo-acoustic tomography (PAT)

In PAT a laser pulse is also sent in to the tissue, experiencing the same propagation losses to reach a certain depth as given by Eq. (1), and is absorbed in the same way in the tissue. The techniques differ however, in the way the absorption is detected. For PAT the absorption of energy that occurs in a particular region creates a pressure wave emanating from that point, due to rapid thermal expansion. This pressure wave can then be detected at the surface of the tissue using acoustic microphones. We again consider a signal absorption path distance of $d = 4.5$ mm, as explained in subsection 2.2. The energy absorbed per unit area of the region of interest, $\Delta E/A = \phi \cdot (1 - e^{-\mu_a d})$, gives rise to a temperature increase:

$$\Delta T = \eta \frac{\Delta E}{V \rho C_v} \approx \eta \frac{\Delta E}{A} \cdot \frac{1}{d \rho C_v}, \quad (4)$$

where η is the fraction of absorbed energy that goes into heating, and ρ and C_v are the density and the specific heat capacity of tissue respectively, taken to be similar to those of water. The rapid heating causes a pressure increase that can be calculated from the bulk modulus, K_T , and the thermal expansion coefficient, β :

$$\Delta P = \beta K_T \cdot \Delta T \quad (5)$$

The process depends in total on four material parameters expressed together as the Grüneisen parameter, $\Gamma = \beta K_T / \rho C_v$, in papers with similar forms of the PAT signal [17]. From this region of interest where the pressure was generated, the now acoustic signal has to travel out to the surface in order to be detected by microphones, and in this process the wave expands, losing pressure amplitude approximately linearly with distance [18].

The pressure signal at the surface must now be compared with the various noise sources. If a resonant detector is used, there are approximately equal contributions from thermal and detector noise, which in total can be modeled by the following expression for the noise equivalent pressure (NEP) [18]:

$$NEP = \sqrt{k_B T (1 + F/\eta) Z / A_{det}} \quad (6)$$

where k_B is Boltzmann's constant, and where we have used the following parameter values (motivated in ref. [18]): temperature $T = 300$ K, preamplifier noise factor $F = 2$, detector efficiency $\eta = 0.5$ (-3 dB achievable for resonant detectors), specific acoustic impedance of tissue/water $Z = 1.5 \cdot 10^6$ Pa·s/m, and detector area $A_{det} = 1$ cm², same as for the UOT case above. This gives

a NEP of approximately $20 \mu\text{Pa}/\sqrt{\text{Hz}}$. In contrast to UOT, where any temporal characteristics give the same CNR, in PAT a scheme with short pulses is more beneficial [19] due to the need to rise above the thermal noise floor. This means the pulse energy is set at the pulsed medical safety limit, and within the 250 ms single-shot duration three such pulses can be used at the rate corresponding to the allowed average power. The detection bandwidth, B_W , of the resonant detector is taken to be the same as the one used for the US pulse in UOT, which is 2 MHz. This gives the total background noise pressure for PAT, $P_{\text{noise}} = \text{NEP} \cdot \sqrt{B_W}$, and note that this is the best that can be achieved in the sense that only fundamental noise sources like thermal noise are included. Similar to the case for UOT (see Sec. 2.3), calculations are performed for two regions with different absorption coefficients. The ability to distinguish those regions is given by the pressure contrast between them compared to the noise:

$$\text{CNR}_{\text{PAT}} = \frac{P_{\text{signal}} - P_{\text{baseline}}}{P_{\text{noise}}} \quad (7)$$

Since PAT can obtain images from multiple regions simultaneously, it is not necessary to divide the medically allowed power between the regions as in the UOT case.

3. Results and discussion

The Matlab code, containing our core calculations used to generate the figures in this section, is available online as Supplementary information (Code 1) [39].

A central question is to analyze how the contrast-to-noise ratios, given in Eqs. (3) and (7) respectively, depend on the imaging depth in tissue. Our calculation results depend on the specific example and here we have chosen to analyze whether it is possible to measure the oxygenation level of the heart under optimal conditions in real time. In Fig. 2 we have plotted the CNRs as a function of imaging depth, i.e. the shortest distance from the region of interest to the tissue surface (r in Fig. 1). The shaded area for each curve correspond to an interval of absorption coefficient differences, $\kappa = \Delta\mu_a/\mu_{a,\text{baseline}}$, going from 0.5% up to 50% of the baseline value. The baseline of the contrast measurement corresponds to a tissue region close to the signal one.

We now briefly give the conditions for the calculations, for a more detailed discussion see Sec 4. The muscle tissue in front of the heart is represented using a reduced scattering coefficient of $\mu'_s = 5 \text{ cm}^{-1}$, and an absorption coefficient of 0.2 cm^{-1} . Similar geometrical setups for both techniques are used, with a detection bandwidth of 2 MHz and for UOT a background suppression due to the absorption filters of 60 dB, and another 20 dB from slow light time gating, which should be realistically achievable. The spatial resolution is 3 mm and the heart is covered by 30 such regions in 250 ms, while staying below the medical safety limits.

As can be seen from the figure, PAT can reach about 3 cm into tissue before the CNR drops below 1 for resolving the largest differences ($\kappa = 50\%$) between absorption coefficients. The corresponding value for UOT is twice as deep at about 6 cm, making it possible to reach the front of the heart for most adults [1]. In particular, the reachable areas of the heart include the left anterior descending artery, which is the most common place for heart ischemia. In addition, also for moderate depths of about 2 cm where both techniques are valid, we note that the CNR for UOT is 2-3 orders of magnitude larger than for PAT. The separation between the input and the detector for UOT, r_b in Fig. 1, is best chosen to match the expected depth and has here been set to 4 cm. This choice also limits the achievable signal level for much smaller depths and is what limits the UOT signal in the few mm range. Although this is largely irrelevant as the CNR is already 10^2 or higher.

The main reason for the higher CNR of UOT at larger depths is the fact that the optical detection employed by UOT can be made shot-noise limited, and that the optical background suppression is highly efficient. For the intermediate depths relevant to our situation, UOT thus scales better. However, if substantially higher imaging depths were possible, PAT would eventually scale better.

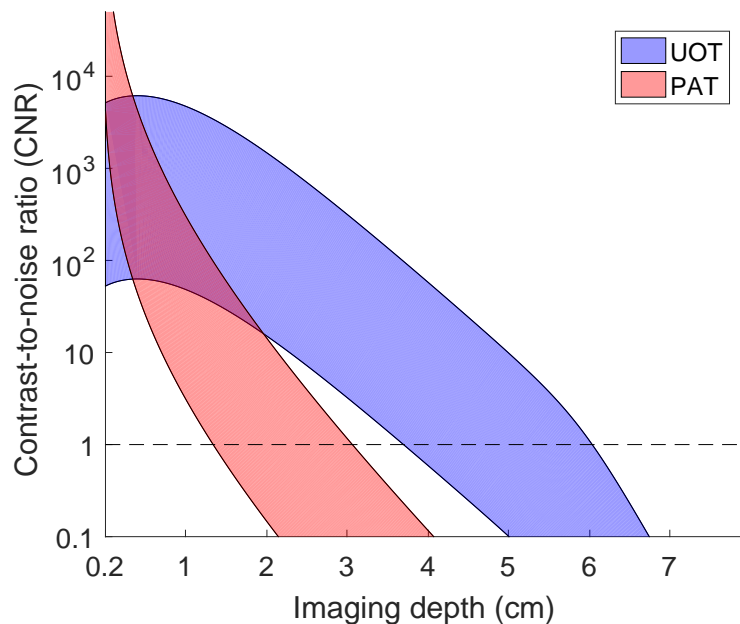


Fig. 2. CNR for a range of absorption coefficient differences plotted as a function of tissue imaging depth, given a real time measurement duration of 250 ms. The contrast is taken between a signal tissue region and a nearby baseline region, with a slightly different absorption coefficient. The area for each curve corresponds to changes in the absorption coefficient (e.g. due to changing oxygenation) varying as percentage of the baseline value from $\kappa = 0.5\%$ (bottom of the area) up to $\kappa = 50\%$ (top of the area). The reachable depth for UOT is approximately twice that for PAT, which allows the front of the heart to be reached. It would also be possible to extend the depth even further using wave-front shaping techniques. For other details see the text.

This is due to the fact that for long enough propagation distance the exponential scaling with the attenuation coefficients for the light will overtake the other sources of signal loss. For PAT, propagation in light form occurs only during the travel towards the region of interest (since the outwards travel is as sound), but for UOT the signal is carried as light also on the way back out from the measurement region. That being said, utilizing this potential for PAT appears difficult since our calculations have already made use of optimal conditions and only fundamental noise sources, such as thermal noise.

Since the y-axis in the figure is logarithmic, most moderate changes to the setup, such as changes to geometry or detector efficiencies, only have small impact on the imaging depth. The largest parameter dependence is found in the tissue losses from the scattering and absorption coefficients since they enter exponentially. Variations to both have similar effects; doubling any of them reduces the depth by about 1.5 cm for UOT, and cutting any one of them in half extends the UOT depth by about 1.5 cm. For PAT the corresponding changes are ± 0.5 -1 cm in either direction.

A necessary requirement for being able to distinguish a certain absorption difference, $\Delta\mu_a$, is that the CNR is above one. Figure 3 shows where this border occurs for the two techniques. In addition, the y-axis on the right-hand side also indicates the corresponding resolution of the oxygen saturation of blood. As was discussed in Sec. 2, Eq. (2) shows an approximate 1:3 relation between $\Delta\mu_a/\mu_a$ and the resolution of oxygen saturation. Furthermore, an absolute value of the oxygen saturation can be obtained by using a second laser color as a reference for

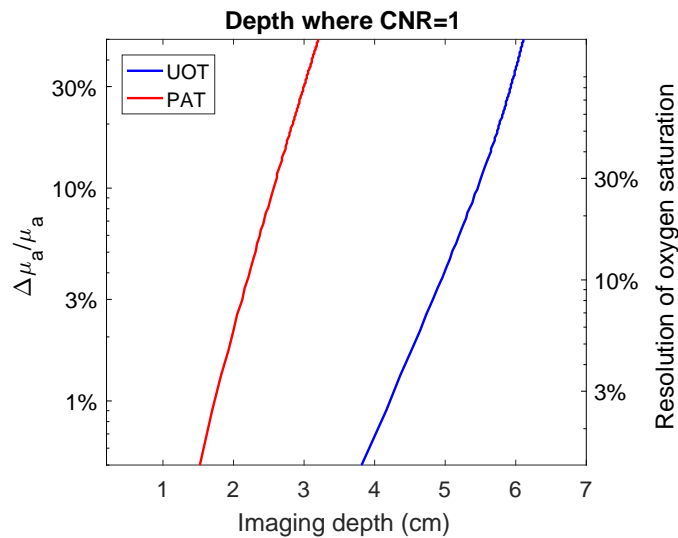


Fig. 3. Difference in absorption coefficient between two volume elements as a function of depth, under the condition that $\text{CNR} = 1$ for UOT and PAT. The data plotted in Fig. 4 can be used to see that a given relative change of the absorption coefficient corresponds to a three times as large relative change in blood oxygenation. The resolution of the oxygenation is displayed as the right-hand y-axis, and could be made into an absolute measurement of oxygenation by the use of a reference second laser color.

obtaining all common unknown factors. In case of full heart attacks, almost all Hb becomes deoxygenated in the affected area of the heart muscle, and the signal should be readily detectable by UOT. To detect less severe lack of oxygen, e.g. early stages of angina, a higher resolution of the saturation levels would be required, limiting the possible depth.

In terms of potential improvement of these results, both techniques could reach deeper by increasing the detector area, since the CNR in both cases scale with the square root of the area. This can be experimentally challenging, but probably less so for PAT, since the microphone detectors are simpler in construction compared with the UOT optical filters plus detectors. As for reducing the noise, in case of PAT, there is no further improvement for in vivo situations, since the current results are based on the fundamental and unavoidable thermal noise. For UOT, the background could be further suppressed by improving the spectral filters beyond the values used here. While simulations show that several orders of magnitude higher suppression may be possible it has not been experimentally verified. Furthermore, the gain from this is limited since the main restriction for UOT (and for PAT) is the low photon count of the signal that survives the attenuation through the tissue, and reducing the background does not change this. As an example, if filters with an additional three orders of magnitude suppression were available, the maximum depth would only increase by less than 1 cm. At the same time, filters with two orders of magnitude less suppression reduces the maximum depth by about 1 cm. This means that neither the technique nor our results are sensitive to moderate changes of the filter attenuation. It is also important to remember that all presented results carry the assumption that all 30 measurement regions can be updated in real time, i.e. every 250 ms. One can obviously improve the CNR by averaging for a longer time, which is the case for many of the experimental results found in the literature. Although, while averaging improves the CNR, it only provides a limited possibility to extend the imaging depth, since it does not affect the exponential scaling. As an example, by averaging the signal for 5 minutes (300 times), the depth can be extended by

approximately 1 cm for both techniques.

The highest impact on improving the reachable depth, for both techniques, would be any method of lowering either the absorption or the scattering coefficient. Both parameters could be changed slightly by using a different wavelength, even though the current results are already within the tissue optical window. However, note that PAT has a smaller improvement from lowering the absorption coefficient than UOT for two reasons. Firstly, as mentioned above PAT is only affected by light attenuation while propagating towards the region of interest, and secondly, PAT relies on the absorption process to create the thermal expansion that leads to the acoustic wave. If the absorption is too low the sound amplitude would be hidden in the thermal acoustic background noise. The most promising strategy for increasing the depth appears to be to significantly lower the impact of the scattering coefficient by involving methods of wave-front shaping, e.g. using phase conjugation or feedback schemes. Such schemes are described in more detail in e.g. Ref. [20] with references therein, and also note that the rare-earth systems suggested as filters here can also be utilized as phase conjugators for this purpose [21].

4. Implementation considerations

In this section we motivate our choices of the absorption and scattering coefficients of tissue and the achievable background suppression in the UOT case, as well as give details of the rare-earth filters required for implementation.

4.1. Absorption and scattering in tissue

Different tissue types have different absorption and scattering coefficients. Thus, while most of the analysis in this paper is generally valid, the results presented in Sec. 3 require specific coefficients to be selected and here the chosen example is measuring the oxygenation level of the frontal part of the myocardial tissue. The shortest path to this region is between or below the ribs through the front of the chest, which consists primarily of muscle tissue. In Fig. 4, the absorption coefficients of the important constituents are plotted.

The specific wavelength selection will be discussed in the next subsection, but within the tissue optical window below 900 nm used here the absorption contributions from water and lipids are negligible. In this case the absorption of muscle tissue comes almost exclusively from oxy- and deoxygenated hemoglobin (Hb). Relevant values of volume fraction of blood in this tissue vary between different sources, but are typically a few percent. For instance, 4 percent blood content (used in the figure) is consistent with several *in vivo* measurements of absorption in muscle tissue [22–24]. Muscle tissue could also include other absorbing components such as connective tissue and fat, as well as myoglobin. Myoglobin has a similar contribution to the absorption as hemoglobin, and all cited references have used *in vivo* techniques, which do not distinguish these elements such that a realistic average tissue is directly obtained. In particular, all measured hemoglobin concentrations may simply be interpreted as an effective hemoglobin + myoglobin absorption [25, p. 479], since they are very similar also in their wavelength dependence. Scattering in tissue occurs predominantly in the forward direction, which to some extent lessens the effect of scattering. This has already been taken into account in the use of the reduced scattering coefficient, sometimes called the transport scattering coefficient. Ref. [26] includes an overview of measurements of scattering parameters in this reduced form, and choosing an average of values related only to measurement in muscle tissue we find a reduced scattering coefficient, μ'_s , of approximately 5 cm^{-1} for the relevant wavelengths. Although note that while the spread of measured values are small for individual studies, such as Ref. [27], meta studies such Ref. [26] reveal larger spreads. This appears to be at least in part due to varying measurement techniques and conditions, constituting a source of uncertainty.

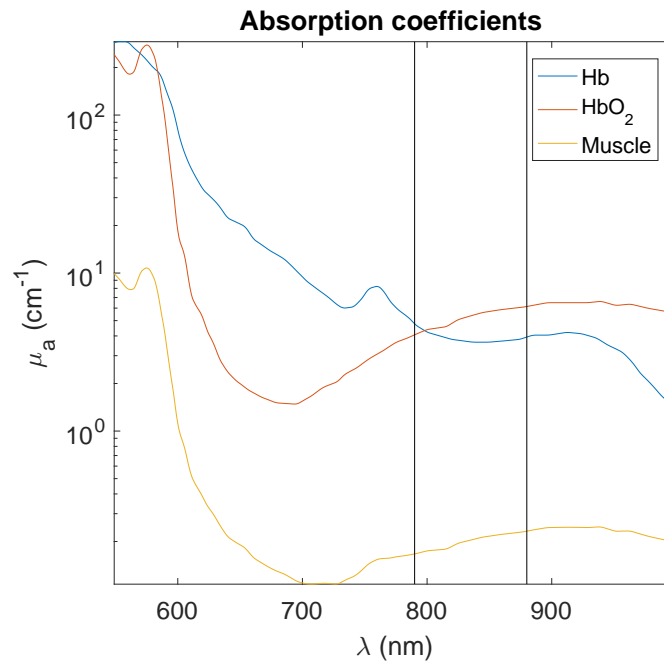


Fig. 4. Absorption coefficients for oxy- and deoxygenated Hemoglobin in full blood (100%), which are the main contributors to absorption in muscle tissue below 900 nm. The curve for muscle tissue represents a realistic mixture with 4% blood and an average of 85% oxygen saturation. The two vertical black lines demonstrate the wavelength 790 nm and 880 nm respectively, where suitable rare-earth-ion filters are available.

4.2. Slow light filters based on rare-earth ions

In UOT the unshifted background light is typically much stronger than the information carrying signal. In order to detect only the small useful part, a filter with a very narrow frequency transmission range has to be used. It should be narrower than the ultrasound frequency (3 MHz) and simultaneously have a very high ratio of attenuation to transmission. Optical Fabry-Perot cavities can be sufficiently narrow, but they only transmit a single spatial mode, making them extremely angle-selective. Since the output light from the highly scattering tissue generally exits in arbitrary directions, cavities are very inefficient filters for this application. Another way of achieving a sharp transmission window is to use narrow atomic absorption lines, such as those found in rare-earth ions in cryogenic temperatures. For these, linewidths down to about 100 Hz have been demonstrated for several species [28, 29], and filters made out of these may have solid angles of acceptance of nearly 2π . Optical pumping sequences can readily be employed to create a filter tailored for the needs of a particular UOT application [30]. Many rare-earth isotopes have several very long-lived nuclear spin states, and hole-burning sequences with laser pulses can empty very narrow frequency intervals for demonstrated durations up to 20 days in some materials [31]. At the same time, the performance of the filter is not related to the phase of the light in any way, which makes them completely immune to speckle decorrelation due to tissue movement. Rare-earth ion spectral tailoring requires liquid helium temperatures. However, this can be achieved without a need for cryogenic liquid supply by using closed-cycle cryostats available at reasonable cost and size. Light can be lead to the crystal by e.g. a large area multi-mode fiber or other optical light guides with an opening in a handheld probe in contact with the tissue surface, similar to how conventional ultrasound systems work today.

In a previous demonstration of UOT [12], a rare-earth filter was implemented using Praseodymium (Pr) ions to achieve a suppression ratio of 30 dB. Later results have demonstrated up to 63 dB in the same material for frequency separations of 10 MHz [32] and 53 dB for as close as 2 MHz separations [33]. By absorption alone in a single crystal it is difficult to achieve even higher attenuation ratios, due to polarization effects in the host material [34]. Although, such effects could be mitigated e.g. by using multiple crystals in a row with different orientations of the birefringent axes, as has been demonstrated for quantum memories [35]. However, another advantage with spectrally tailored atomic absorption filters is that a compound time gating attenuation can be achieved in addition to that from the absorptive attenuation. This is because of a slow light effect inherently arising from the strong dispersion of such narrow features in these materials [36]. The group velocity of a light pulse can be expressed as [36, 37]: $v_g = 2\pi\Gamma_{hole}/\alpha$, where the FWHM of the burnt spectral hole, Γ_{hole} , can typically be made narrower than 1 MHz and the absorption coefficient outside of the hole, α , can often be about 50 cm^{-1} , which gives a group velocity of light of about 1000 m/s. For a 1 cm long crystal this gives a time delay of about $10\text{ }\mu\text{s}$ to pulses in the transmission window, which can then with a good suppression be distinguished from the small fraction of non-delayed light that passes through the 50-60 dB absorptive part.

The peak absorption of a crystal increases with defect ion concentration, but only up to a certain point where instead increased crystal distortions lead to inhomogeneous broadening effects. This limit could be circumvented using stoichiometric crystals, where the active ions are a part of the host instead of being a defect, and where absorption coefficients $>1000\text{ cm}^{-1}$ have been suggested [38].

For applications in medicine it is desirable to operate at a wavelength in the so called tissue optical window, approximately between 650 to 900 nm, where the absorption is at a minimum. In order to use rare-earth filters, one thus have to find rare-earth species that have a matching transitions in this regime. Two promising candidates for this is Thulium (Tm) and Neodymium (Nd), at wavelengths of about 790 and 880 nm respectively. As can be seen in Fig. 4, the dependence on oxygenation level is larger for 880 nm, which would be the primary signal wavelength. A co-signal from the second wavelength could then be used to calculate all common loss factors, enabling an absolute value of the oxygenation to be obtained. It may also be possible to identify further useful rare-earth transitions, in particular Tm may have other lines around 700 nm where the total absorption is lower. Note also that two or more different rare-earth ions may be co-doped into the same physical crystal. A potential drawback of the rare-earth filters is that the choice of wavelength is limited to where there are rare-earth absorbers. There are at least two within the tissue window, as mentioned, but if there are several chromophores that cause differences in absorption, there could be an advantage to use even more wavelengths than two.

5. Conclusions

We have used a simple model based on the diffusion equation to calculate the expected contrast-to-noise ratios for two important non-invasive medical imaging techniques, UOT and PAT. Our results suggest that UOT could reach further into tissue than PAT, and UOT also obtains a substantially higher CNR at intermediate depths. In particular, UOT could reach the front side of the myocardial tissue with sufficient absorption contrast to resolve the blood oxygen saturation, giving a real-time non-invasive method to verify a potential heart infarction or angina. In order to experimentally realize the full potential of UOT, we suggested using rare-earth slow light filters, where a proof-of-principle demonstration with good results has already been made and where further improvements are available. It is also worth pointing out that even if we chose one specific example here, we believe that UOT with the rare-earth filters should be the better technique in a more general setting as well, as long as the target depth is deep enough. Thus, UOT appears to be a promising technique that would be interesting to study further. Given the substantial part

of emergency patients that have issues potentially related to lack of oxygen (ischemia), it could have a significant impact on some directions of future medical imaging techniques.

Funding

Swedish Research Council, Lund Laser Center (LLC), through a project grant under the Lund Linneaus environment, the Knut and Alice Wallenberg Foundation, and the Science Foundation Ireland.

Acknowledgments

The authors would like to thank Prof. Lars Edvinsson, at the Lund University Hospital, for useful discussions, and Dr. Jacqueline Gunther for observant code checking.

Disclosures

The authors declare that there are no conflicts of interest related to this article.